

Light-scattering characterization of transparent substrates

Myriam Zerrad, Carole Deumié, Michel Lequime, Claude Amra, and Mike Ewart

Angle-resolved light scattering has been used for decades to quantify the surface roughness of optical components. However, because this technique is affected by the contribution of both interfaces of the sample, it cannot be applied to transparent substrates. We show how to overcome this issue and apply these principles to the characterization of superpolished samples. © 2006 Optical Society of America
OCIS codes: 120.5820, 120.6660.

1. Introduction

Far-field light scattering has been extensively studied these past decades^{1–10} as a technique for surface-roughness characterization. In the case of opaque samples, using both angle-resolved-scattering (ARS) measurements and a specific electromagnetic theory, we can deduce the surface-roughness spectrum, which once integrated provides a root mean square of the roughness in the optical bandwidth. Roughness values can currently be measured down to 0.1 Å, with a relative accuracy of approximately 3%.

However, this technique is valid mainly in the case of opaque substrates. When the substrates are transparent, scattering from both interfaces is simultaneously collected by the receiver in the far field, so that additional discrimination is required.^{11,12} In this paper we present the modifications we performed to the experimental setup, which are based on geometrical considerations, to overcome this issue.

2. Characterization of Opaque Substrates

For a single surface whose irregularities are assumed to be much smaller than the illumination wavelength, a simple relationship issued from first-order theory^{1,2,6,13–15} allows us to determine the surface

properties from the angular data of the scattering pattern:

$$I(\theta, \phi) = C^\pm(\theta, \phi) \gamma(\theta, \phi), \quad (1)$$

where θ and ϕ are the normal and polar angles, respectively, that describe a scattering direction in the far field (as illustrated in Fig. 1) and $C^\pm(\theta, \phi)$ is an optical factor that takes into account the material index, polarization, and wavelength. C^\pm is defined for normal illumination and natural light in reflection (C^-) or in transmission (C^+) by

$$C^-(\theta, \phi) = C^-(\theta) = \frac{1}{2} \left(\frac{2\pi n_0}{\lambda} \right)^2 [\cos^2 \theta_0 |q_s|^2 + |q_p|^2], \quad (2)$$

$$C^+(\theta, \phi) = \frac{1}{2} \left(\frac{n_s^3}{n_0} \right) \left(\frac{2\pi}{\lambda} \right)^2 [\cos^2 \theta_s |q_s|^2 + |q_p|^2], \quad (3)$$

with

$$q_s(\theta) = j \left(\frac{2\pi}{\lambda} \right) 2n_0(n_0 - n_s)(n_0 \cos \theta_0 + n_s \cos \theta_s)^{-1},$$

$$q_p(\theta) = j \left(\frac{2\pi}{\lambda} \right) 2n_0(n_0 - n_s)(n_0 / \cos \theta_0 + n_s / \cos \theta_s)^{-1}, \quad (4)$$

$$n_0 \sin \theta_0 = n_s \sin \theta_s. \quad (5)$$

The roughness spectrum $\gamma(\theta, \phi)$ of the surface is

M. Zerrad (myriam.zerrad@fresnel.fr), C. Deumié, M. Lequime, and C. Amra are with Institut Fresnel, Unité Mixte de Recherche-CNRSTIC 6133, Ecole Généraliste d'Ingénieurs de Marseille, Université Paul Cézanne Aix-Marseille I, Domaine Universitaire de St. Jérôme, 13397 Marseille Cedex 20, France. M. Ewart is with WZW Optic AG, Postfach 42, Mühlesteinstrasse 12, 9436 Balgach, Switzerland.

Received 1 March 2005; revised 25 July 2005; accepted 13 August 2005.

0003-6935/06/071402-08\$15.00/0

© 2006 Optical Society of America

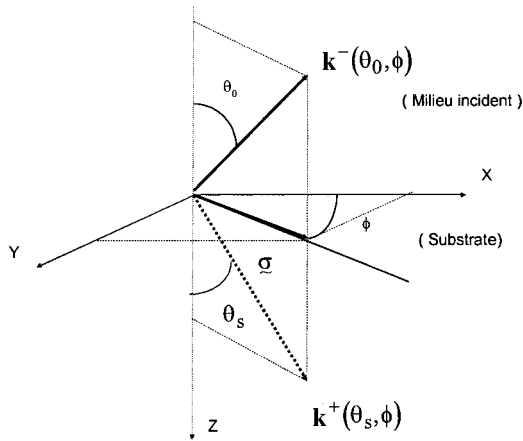


Fig. 1. Scattering angles.

given by

$$\gamma = \frac{4\pi^2}{S} |\hat{h}(\sigma)|^2, \quad (6)$$

where \hat{h} is the Fourier transform of the surface profile $h(\mathbf{r}) = h(x, y)$; S is the illuminated area on the sample, and $\sigma = 2\pi(\sin \theta/\lambda)\{\cos \phi; \sin \phi\} = 2\pi\nu$, where ν is the spatial frequency. With Eq. (1) the spectrum can be extracted from measurements, which allows us to quantify the roughness value δ , or root mean square, in the optical bandwidth:

$$\delta^2 = \frac{1}{S} \int h^2(\mathbf{r}) d\mathbf{r} = \int \gamma(\sigma) d\sigma, \quad (7)$$

with $d\mathbf{r} = dx dy$ and $d\sigma = d\sigma_x d\sigma_y$.

These results have been extensively published in the past.^{1,2,14,16}

3. Case of Transparent Substrates

In the case of transparent substrates, both substrate interfaces give light scattering, as illustrated in Fig. 2.

As shown in Fig. 3, the incident light is first scattered by interface 1 in reflection (I_1^-) and in transmission (I_1^+).

If γ_1 is the roughness spectrum of interface 1 and C_1^- and C_1^+ are the factors defined in Eqs. (2) and (3) in reflection and transmission, respectively, we can write

$$I_1^- = C_1^- \gamma_1, \quad (8)$$

$$I_1^+ = C_1^+ \gamma_1. \quad (9)$$

I_1^+ will then be reflected on interface 2 and transmitted through interface 1 before being measured in the reflected half-space. So, as seen from the detector, the contribution I_1^t of the light scattered in transmission

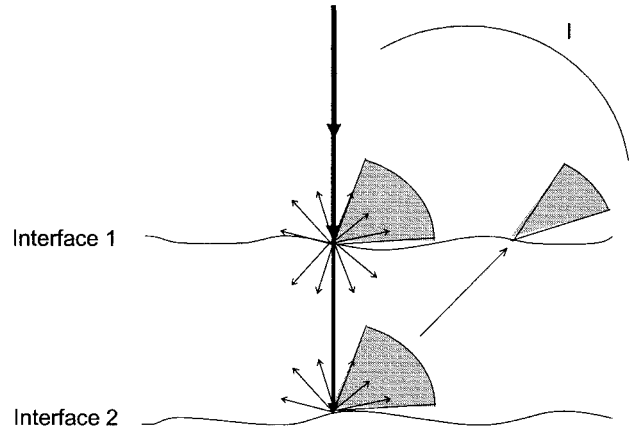


Fig. 2. Light scattering in transparent substrates.

through interface 1 is

$$I_1^t = R\beta C_1^+ \gamma_1, \quad (10)$$

where R is the angular reflectance and β is the angular diffuse transmittance of the glass-air interface defined by^{6,11}

$$\beta = T \left(\frac{n_0}{n_s} \right)^2 \frac{\cos \theta_0}{\cos \theta_s}. \quad (11)$$

On the other hand, we can consider the light transmitted through interface 1 and scattered by interface 2 (Fig. 4) with intensity I_2 . If we define the incident intensity on interface 1 as I_0 , taking into account the multiple reflections inside the substrate, the incident intensity on interface 2 is

$$I_i = \frac{T}{1 - R^2} I_0, \quad (12)$$

so that we have

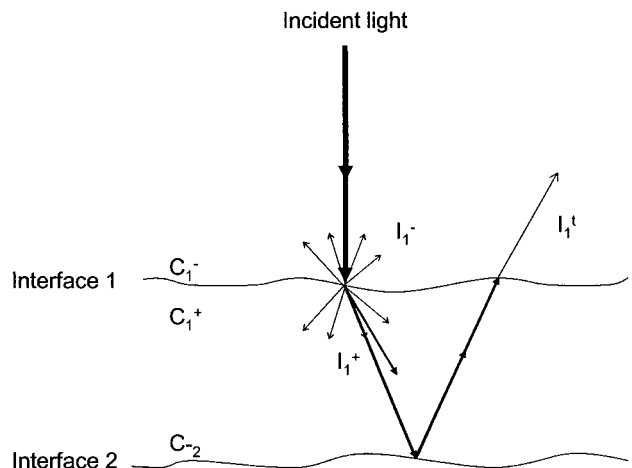


Fig. 3. Light scattered by interface 1 in a transparent substrate.

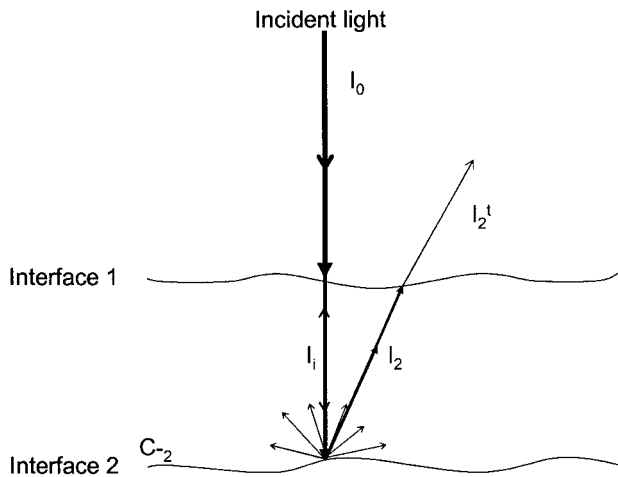


Fig. 4. Light scattered by interface 2 in a transparent substrate.

$$I_2 = \frac{T}{1 - R^2} C_2 \gamma_2. \quad (13)$$

Then I_2 is transmitted through interface 1. So the contribution I_2^t of the light scattered by interface 2 is

$$I_2^t = \beta I_2. \quad (14)$$

Finally, the scattered light coming from both interfaces and measured in the reflected half-space is given by

$$\begin{aligned} I(\theta) &= I_1^-(\theta) + I_1^t(\theta) + I_2^t(\theta) \\ &= C_1^- \gamma_1 + R\beta C_1^+ \gamma_1 + \frac{T}{1 - R^2} \beta C_2^- \gamma_2. \end{aligned} \quad (15)$$

If the sample is studied in the same way as an opaque sample with a single interface reachable, a roughness

spectrum γ can be deduced as follows:

$$\gamma(\theta) = \frac{I(\theta)}{C_1^-(\theta)}, \quad (16)$$

where $C^-(\theta) = C_1^-(\theta)$.

So the equivalent roughness spectrum γ_{eq} deduced from the I measurement for interface 1 is in fact

$$\begin{aligned} \gamma_{eq} &= \frac{I(\theta)}{C_1^-(\theta)} \\ &= \frac{I_1^-(\theta) + I_1^t(\theta) + \beta I_2(\theta)}{C(\theta)} \\ &= \gamma_1 + R\beta \frac{C_1^+(\theta)}{C_1^-(\theta)} \gamma_1 + \frac{T}{1 - R^2} \beta \frac{C_2^-(\theta)}{C_1^-(\theta)} \gamma_2. \end{aligned} \quad (17)$$

So we can see that the roughness spectrum γ deduced for interface 1 is different from both γ_1 and γ_2 and that it is not an obvious combination of γ_1 and γ_2 . In Fig. 5 the equivalent spectrum γ_{eq} is plotted for two spectra simulating γ_1 and γ_2 for the case in which $\gamma_1 = \gamma_2$. This shows that in the case of transparent substrates, the spectrum deduced from a classical measurement contains an error due to the second-interface contribution that is not negligible.

So, in the case of transparent substrates, to provide an adequate sample characterization, one must discriminate between the light scattered by both interfaces. Several solutions were proposed a few years ago¹⁷ with limited success, based on simultaneous data analysis in the reflected and transmitted half-spaces. We propose here a simple solution based on geometrical considerations, which permits the isolation of the scattering from each face.

4. Experimental Setup and Theoretical Investigation

The measurements were carried out on a scatterometer developed at the Fresnel Institute and were

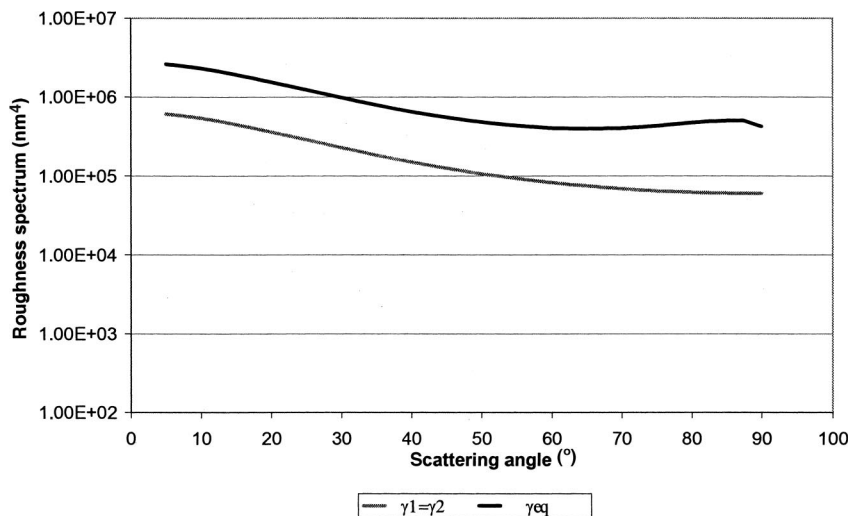


Fig. 5. Difference between real and equivalent spectra.

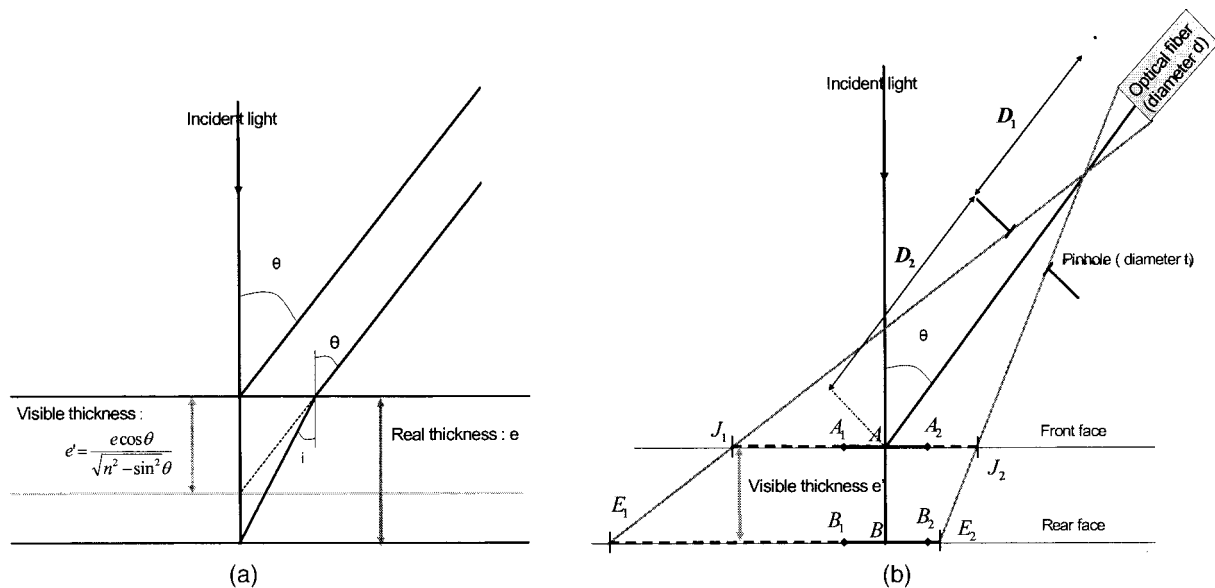


Fig. 6. Side view showing the separation of both faces using the geometrical approach. (a) Definition of the equivalent thickness of the sample as a function of the scattering angle. (b) Visualization of the areas illuminated and measured by the scatterometer on each interface of the sample.

based on the collection in the far field of scattered light by a detector placed on a rotating arm.¹⁵ We now describe those modifications realized to perform the present study.

An elementary optical system was added on the rotating arm, between the sample and the collecting optical fiber. This optical system is defined in the simplest way by the fixation of a pinhole in the direction of the measured direction θ , as illustrated in Fig. 6. The eligible parameters are D_1 and D_2 , the distance from the hole to the sample and from the hole to the optical fiber, respectively, with t the diameter of the hole. Adjustment of these parameters allows interface discrimination optimization.

We can see in Fig. 7 that using this optical system allows an area S_1 to be fully captured by the scatterometer on the front interface of the sample, and in the

same way, an area S_2 can be fully captured by the captor on the rear sample interface. S_1 and S_2 can be defined as a function of parameters t , D_1 , and D_2 . In other words, the optical fiber can collect only light scattering that originates from S_1 and S_2 . These surfaces are ellipsoidal, and their areas vary with angle θ . Therefore all parameters must be chosen to reduce or increase the ratio S_1/S_2 , so that one surface can be measured regardless of the other. To go further we define the capture ratio by

$$C = \frac{S_2 \cap \Sigma_2 (\text{face 2})}{S_1 \cap \Sigma_1 (\text{face 1})} \quad (18)$$

where Σ_1 and Σ_2 are the illuminated areas on each interface, (S_1 and S_2) are the areas measured by the captor on each interface, and $S_1 \cap \Sigma_1$ is the area common between S_1 and Σ_1 . This ratio permits the

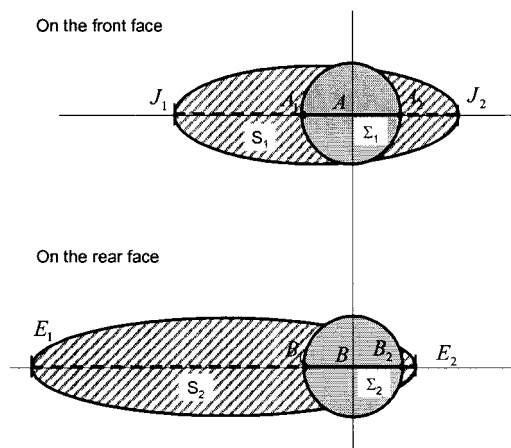


Fig. 7. Top view showing the separation of both faces using the geometrical approach.

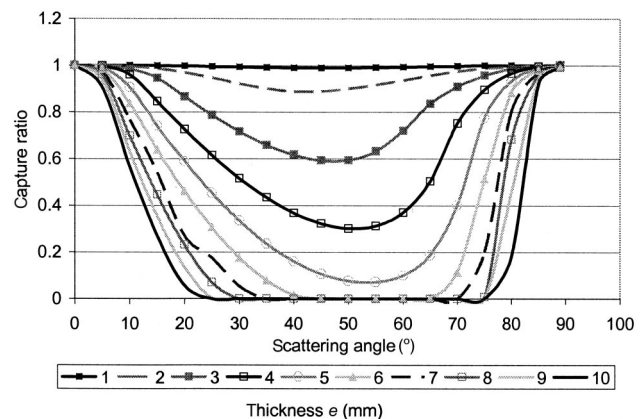


Fig. 8. Capture ratio for different sample thicknesses.

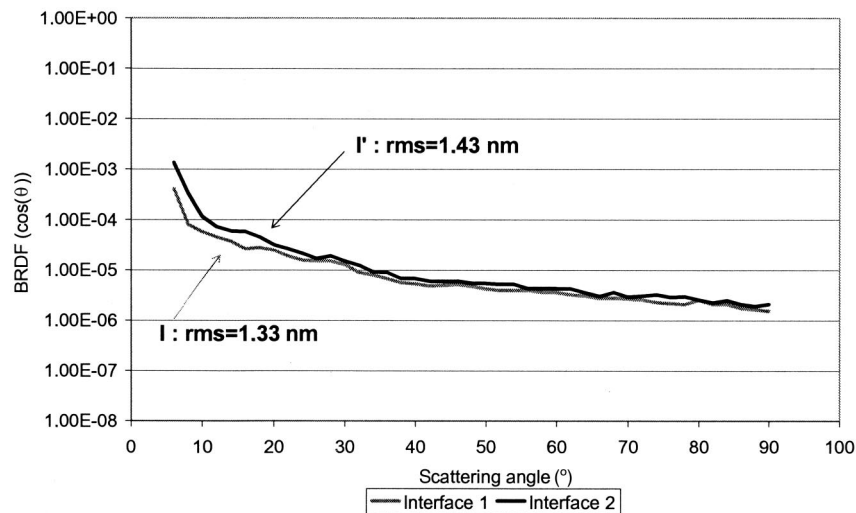


Fig. 9. Intensity scattered I by a superpolished transparent substrate measured without the separation system. BRDF, bidirectional reflectance distribution function.

quantification of the amount of scattering from interface 2, which is simultaneously collected with the scattering from interface 1. All parameters in Fig. 6 can be calculated by trigonometric relations and numerical implementations. The visible areas depend on the thickness sample and, more precisely, on the equivalent thickness e' , which is

$$e' = \frac{e \cos \theta}{(n^2 - \sin^2 \theta)^{1/2}}. \quad (19)$$

In Fig. 8 the capture ratio is numerically calculated as a function of the scattering angle θ for different values of the sample thickness. These results were obtained with $D_1 = D_2 = 20$ cm and $t = 1$ mm.

It must be noticed that the capture ratio equals zero in a limited angular domain, provided that the sample is thick enough. In this case the front inter-

face can be insulated. The same technique can then be used to characterize the other surface (rotation of sample perpendicular to its plane).

5. Application

To validate the technique, we used 9 mm thick optical polish-quality fused-silica samples. Light-scattering measurements were performed first without the separation system (Fig. 9) and then with the separation system (Fig. 10). In this last measurement configuration, when the incident light arrives on interface 1, we measure I_1 . Then the sample is turned and illuminated on interface 2, and I_2' is measured.

On the one hand, we can see a difference in the scattering level, depending on whether the separation system is used. On the other hand, we note that there is a higher intensity gap between the two measurements when the separation system is used.

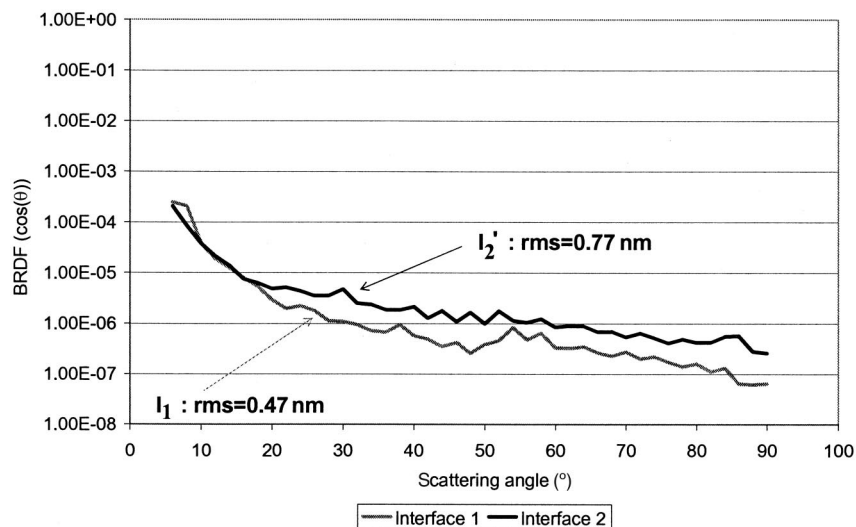


Fig. 10. Intensity scattered I_1 and I_2 by each interface of a superpolished transparent substrate measured with the separation system.

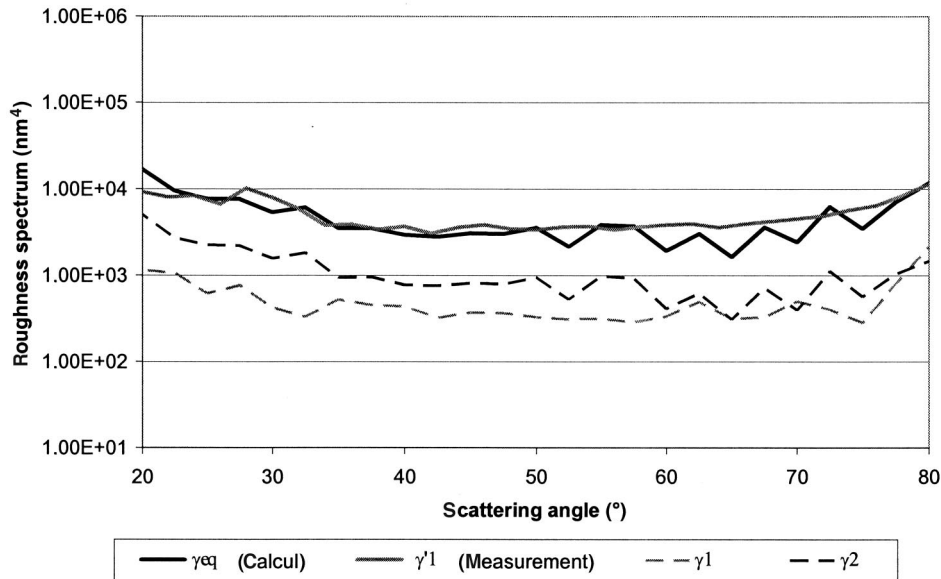


Fig. 11. Calculated and measured roughness spectra (higher spectra values for higher scattering angles are due to the parasite light coming from the sample side).

Let us now see whether the experiment confirms what we saw in Section 4. The roughness spectra γ_1 and γ_2 of interfaces 1 and 2, respectively, were calculated with Eq. (1) from the intensities I_1 and I_2' , respectively, given in Fig. 10 and measured with the separation system. The spectrum γ_1' of interface 1 was deduced from the intensity I measured without the separation system and shown in Fig. 9. In addition, the equivalent roughness spectrum γ_{eq} of interface 1, calculated with Eq. (17), which is expected knowing γ_1 and γ_2 , is plotted in Fig. 11. First, we can see that γ_1 and γ_2 are different from each other and that γ_1 and γ_2 are lower than γ_1' , confirming the results given in Figs. 9 and 10.

Moreover, we notice that the calculated spectrum γ_{eq} has the same level as that of the measured spectrum γ_1' . We can then deduce that the γ_1 and γ_2 spectra are the real spectra of interfaces 1 and 2, respectively.

To finish, we can quantify the roughness values of each interface and compare them with the values that should be obtained in the absence of the separation system. Results are shown in Figs. 9 and 10. In Fig. 9 the two curves correspond to the measurement of the same sample insulated on one interface and then on the other. The curves are nearly the same, with a roughness value close to 1.4 nm. In this case both interfaces are contributing to light scattering, and the result is nearly the same regardless of the illuminated interface. In Fig. 10 we can see that the separation system permits the measurement of the differences between both faces. In this case the roughnesses deduced are 0.47 nm for interface 1 and 0.77 nm for interface 2.

6. Comparison with Atomic Force Microscopy Measurements

The final verifications were performed by atomic force microscopy (AFM). Previous studies^{14,16,18} have

shown that it is possible to predict angular light scattering through the measurement of the surface profile by using microscopic techniques. Toward this end, we use AFM. Equation (1) can be applied. The optical term C is calculated by using the optical parameters (index, wavelength, and polarization),^{1,2} and the roughness spectrum is given by Eq. (6), where the profile h comes from the microscopic measurement. We can see in Fig. 12 the AFM image of another 9 mm thick optical polish-quality fused-silica sample.

However the AFM bandpass (B_{AFM}) must be adjusted to the ARS one (B_{ARS}), since we have

- $B_{ARS}(\lambda) = [\sin \theta_m / \lambda, 1 / \lambda]$ with λ the incident wavelength,
- $B_{AFM}(\Delta x) = [1 / L, 1 / 2\Delta x]$ with L^2 the measured area and Δx the sampling interval.

The parameters we chose are $L = 50 \mu\text{m}$ and $N = 256$, which guarantee an intersection of ARS and AFM bandwidths.^{16,19} Therefore the AFM data can be

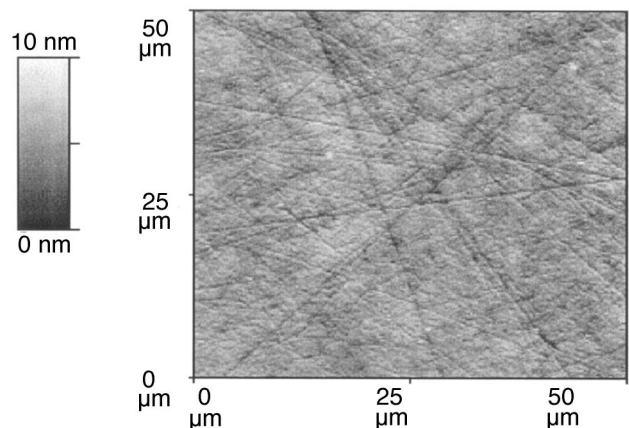


Fig. 12. AFM image of the sample surface.

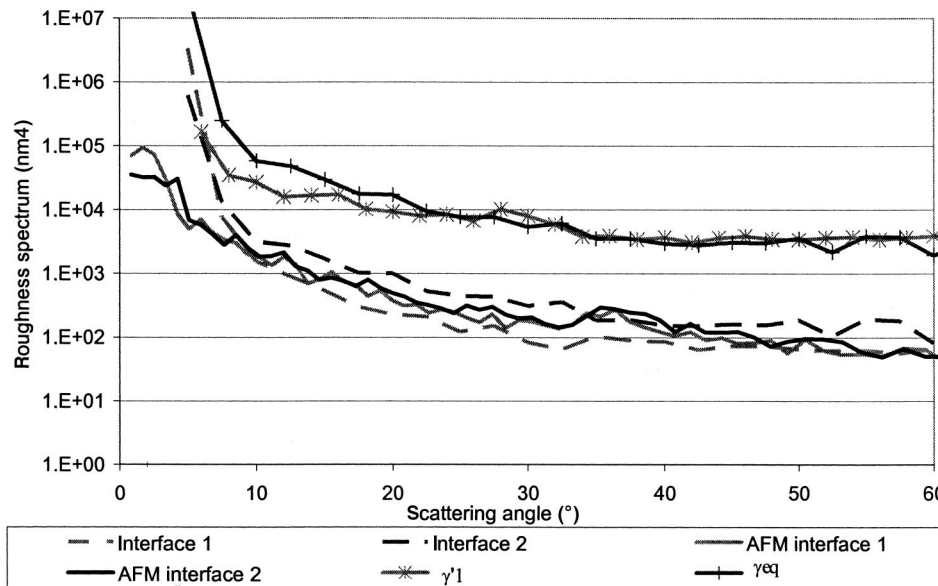


Fig. 13. Comparison between the roughness spectra calculated from the AFM measurements of each interface of the sample and the measured spectra for each interface.

used to calculate the roughness spectrum, and this spectrum is then used in the scattering calculation.

In Fig. 13 we can see that the angular scattering collected from the front and back surfaces is in agreement with the AFM calculation for the same surfaces. Differences still remain but are due to the stationarity of the surfaces at the AFM scale. On the other hand, the measurement performed without the separation system (Fig. 13) yields a roughness spectrum that is very far from the real spectrum.

7. Conclusion

A technique to insulate scattering from each interface of a transparent substrate has been introduced. Such a procedure allows us to characterize the micropolish of each face of a superpolished transparent sample. The results were checked with AFM measurements.

This research was partially supported by the European Union within the framework of the Cooperative Research Action for Technology, Development and Application of Compact Mode-Locked Lasers project.

References

1. C. Amra, "Light scattering from multilayer optics. Part A: Investigation tools," *J. Opt. Soc. Am. A* **11**, 197–210 (1994).
2. C. Amra, "Light scattering from multilayer optics. Part B: Application to experiment," *J. Opt. Soc. Am. A* **11**, 211–226 (1994).
3. J. M. Bennet and L. Mattsson, *Introduction to Surface Roughness and Scattering* (Optical Society of America, 1989).
4. L. Bruel, "Etude comparative de méthodes optiques et mécanique pour caractériser les états de surface. Diffusion de la lumière par les rugosités de surface et inhomogénéités de volume dans les empilements de couches minces," Ph.D. dissertation (Univ Aix-Marseille III, Marseille, France, 1992).
5. P. Croce and L. Prod'homme, "Ecart observé dans l'interprétation des indicatrices de diffusion optique par des

théories vectorielles simples," *J. Opt.*, (Paris) **16**, 143–151 (1985).

6. J. M. Elson, J. P. Rhan, and J. M. Bennet, "Relationship of the total integrated scattering from multilayer-coated optics to angle of incidence, polarization, correlation-length, and roughness cross-correlation properties," *Appl. Opt.* **22**, 3207–3219 (1983).
7. A. Sentenac and J. J. Greffet, "Mean-field theory of light scattering by one-dimensional rough surfaces," *J. Opt. Soc. Am. A* **15**, 528–532 (1998).
8. A. Sentenac, J. J. Greffet, H. Giovannini, and M. Saillard, "Scattering from rough inhomogeneous media: splitting of surface and volume scattering," *J. Opt. Soc. Am. A* **19**, 727–736 (2002).
9. P. Vincent, "Differential method," in *Electromagnetic Theory of Gratings*, Vol. 22 of Topics in Current Physics (Springer-Verlag, 1980), pp. 101–121.
10. A. G. Voronovitch, "Small slope approximation in wave scattering from rough surfaces," *Sov. Phys. JETP* **1**, 65–70 (1985).
11. D. Torricini and C. Amra, "Light scattering to characterize both faces of transparent substrates: embedded and radiative transfer," in *Optical Interference Coatings Proc. SPIE* **2253**, 1117–1130 (1994).
12. M. Zerrad, C. Deumié, and M. Lequime, "Diffusion de la lumière par des substrats transparents: caractérisation d'états de surfaces," poster presented at the Horizons de l'Optique, Toulouse, France, 3–5 September 2003.
13. C. Amra, "First order vector theory of bulk scattering in optical multilayers," *J. Opt. Soc. Am. A* **10**, 365–374 (1993).
14. C. Amra, D. Torricini, and P. Roche, "Multiwavelength (0.45–10.6 μm) angle-resolved scatterometer or how to extend the optical window," *Appl. Opt.* **32**, 5462–5474 (1993).
15. C. Deumié, "Ellipsométrie sur champ diffus et analyse multi-échelle de la microstructure des multicouches optiques: diffusion lumineuse, microscopie à force atomique, microscopie à effet tunnel optique," Ph.D. dissertation (Université Aix-Marseille III, Marseille, France, 1997).
16. C. Deumié, R. Richier, P. Dumas, and C. Amra, "Multiscale roughness in optical multilayers: atomic force microscopy and light scattering," *Appl. Opt.* **35**, 5583–5594 (1996).

17. D. Torricini and C. Amra, "Light scattering to characterize both faces of transparent substrates: radiative and embedded light," in *Optical Interference Coatings* Proc. SPIE **2253**, 1117–1130 (1994).
18. P. Dumas, B. Bouffakhredine, C. Amra, O. Vatel, E. André, R. Galindo, and F. Salvan, "Quantitative microroughness using near field microscopies and optical," *Europhys. Lett.* **22**, 717–722 (1993).
19. C. Amra, C. Deumié, D. Torricini, P. Roche, and R. Galindo, "Overlapping of roughness spectra measured in macroscopic (optical) and microscopic (AFM) bandwidths," in *Optical Interference Coatings*, Proc. SPIE **2253**, 614–630 (1994).